Texture Improvements in the High-Temperature Superconducting $Bi_2Sr_2Ca_1Cu_2O_x$/Ag System via Surface Energy Driven Grain Alignment

by

MARK E. VODHANEL

Submitted to the Department of Physics in partial fulfillment of the Requirements for the Degree of

BACHELOR OF SCIENCE

at the

MASSACHUSETTS INSTITUTE OF TECHNOLOGY

February, 2005 [June 2005]

Signature of Author _____
Department of Physics
January 18th, 2005

Certified by _____
John B. Vander Sande
Cecil and Ida Green Distinguished Professor
Thesis Supervisor, Department of Materials Science and Engineering

Accepted by _____
Professor David E. Pritchard
Senior Thesis Coordinator, Department of Physics

Texture Improvements in the High-Temperature Superconducting $Bi_2Sr_2Ca_1Cu_2O_x$/Ag System via Surface Energy Driven Grain Alignment

By

Mark E. Vodhanel

Submitted to the Department of Physics on
January 18th, 2005, in partial fulfillment of the
requirements for the degree of
Bachelor of Science in Physics

Abstract

The relation between processing, microstructure, and material property was investigated in the high-temperature superconducting $Bi_2Sr_2Ca_1Cu_2O_x$/Ag system. Experiments were based on a theoretical surface energy model proposing enhanced texture of the oxide at the Ag interface after melt-processing. Two classes of samples were processed and compared. Bi-2212 powder was deposited on a thin-foil Ag surface and was melt-processed to yield a 20 ± 10 micron-thick superconducting layer. A subset of these samples were processed with an additional Ag surface pneumatically pressed on top of the superconducting layer before heat treatment. Critical current density (J_c) measurements were performed in liquid helium and we obtained values ranging from 5,900-36,700 A/cm^2. A 3-6 fold increase in J_c for samples with the second Ag interface was observed. X-ray diffraction provided a technique for quantifying grain alignment via the Lotgering factor, and indicated samples with the upper Ag interface possess a higher degree of texturing. Our results support the interfacial energy model that a high degree of texture exists at the Ag surface, and provide clear evidence linking materials processing, superconducting grain alignment, and critical current density. Disparities observed in J_c for similarly processed samples were believed to be a consequence of local regions of alignment and the presence of impurities.

Thesis Supervisor: John B. Vander Sande

Title: Cecil and Ida Green Distinguished Professor, Department of Materials Science and Engineering

Table of Contents

List of Figures

List of Tables

Acknowledgements

The author would like to especially thank Professor John Vander Sande for his countless discussions regarding superconductivity and his general guidance throughout the research process.

Many thanks also to Paulo Ferreira for his support during the early stages of the project.

The author would further like to express gratitude to Yin-Lin Xie and Joe Adario for their technical instruction, and to David Bono for his assistance in measurement setup.

Chapter 1

Introduction

Superconducting materials are characterized by the unique property of zero electrical resistance below a certain temperature and possess the potential for many technological applications. The perfect conductivity property is ideal for the transport and storage of electrical energy. Further, strong magnets can be created from superconducting wires carrying high currents with no resistive energy dissipation. Magnetic Resonance Imaging technology, magnetic levitation high-speed trains, and bending magnets for giant atom-smashing accelerator devices all currently make use of such magnets. The principal problem with these technologies is that the superconductors must be kept in extremely cold conditions to preserve their properties, often requiring an expensive and cumbersome liquid helium cooling system that serves as a severe cost-prohibiting barrier. Our work is part of a larger ongoing investigation of a relatively new class of superconductors discovered within the last twenty years, so-called high-temperature superconductors, which can retain their properties at an economically-viable liquid nitrogen temperature. Large-scale application of these new materials has been limited by low critical current values induced by poor superconductor grain alignment. Our experiment draws upon a theoretical surface energy model proposing improved $Bi_2Sr_2Ca_1Cu_2O_x$ grain alignment at an Ag interface.

Chapter 2

Background Theory

2.1 Superconductivity

The defining characteristic of the superconducting state of matter is the macroscopic property of zero electrical resistivity below a certain critical temperature T_c. This phenomenon was first observed by Kamerling Onnes shortly after he succeeded in liquifying helium in the early twentieth century. As most elemental metals exhibit superconductivity within only a few degrees of absolute zero, this unique state of matter could not be observed until such extreme cold temperatures were achieved. It was later experimentally determined that superconductors possess a second distinct property: the complete exclusion of magnetic flux from within the material.

Neither of the two distinguishing manifestations of the superconductoring state could be explained by classical physics, and it was not until nearly fifty years after Onnes' discovery that a full theoretical treatment of superconductivity was developed. Bardeen, Cooper, and Schrieffer showed with mathematical rigor in 1957 [1] that these two phenomena had very deep quantum and statistical underpinnings in what today is known as BCS theory. The crux of the theory is that electrons form bound Cooper pairs that interact via a lattice vibration as they propagate unimpeded through the material.

The transition from the superconducting state of a material to the normal state is thermodynamically reversible and can be destroyed by raising the temperature of the system above T_c. It was also observed experimentally that a certain critical magnetic field, B_c, or critical current density, J_c, would return the system to its normal state. BCS theory provided an explanation for these properties as well, demonstrating that an energy gap

exists between the normal and superconducting states. This gap is the energetic driving force for the zero electrical resistance property: once the current is in the superconducting state, it is energetically unfavorable to break apart the Cooper pairs, the destruction of which leads to normal electron scattering and electrical resistance. Either of the three critical points, T_c, B_c, or J_c, can be understood as adding sufficient energy to the system to overcome the energy barrier.

Of particular relevance to our work is the critical current point, and we will take a moment to discuss its atomistic origins following a qualitative discussion in Chaddah [2]. A more rigorous treatment can be found in the Campbell and Evetts paper [3]. Typical superconducting pure elements have a sharp transition into the normal state above B_c, where magnetic flux can again penetrate the material and zero resistance is lost. However, certain compound materials, called Type II superconductors, have a more continuous phase transition into a "mixed state" where some magnetic field can penetrate while maintaining zero electrical resistance before entering the normal state. The magnetic flux exists as quantized vortices in these materials. The vortices are arranged in such a way to minimize their free energy, and, as it turns out, the ideal arrangement provides a canceling out of the **B** fields; Maxwell's equations would then imply that curl $\mathbf{B} = 0$. But when a current density **J** flows, curl **B** cannot be zero and the vortices can no longer be arranged in a way to cancel out. The result is a force causing each vortex to move. Vortex motion then creates an electrical field parallel to **J** and hence a finite resistivity. The resistivity rises with increasing **J**, and thus determining the exact location of J_c requires a defining criterion.

2.2 High-Temperature Superconductivity

The discovery of high-temperature superconductivity in 1986 by Georg Bednorz and Alex Müller [4] revived a declining interest in the field due to the seeming impracticality of many low-temperature applications. Their report of $La_{0.85}Sr_{0.15}CuO$ possessing a T_c of 40 Kelvin set off a flurry of research with the ultimate goal of finding a material with a critical point above room temperature. Elemental metals generally exhibit a T_c near 5-10 K, but within a few years of the stunning announcement, many ceramics were discovered to have transitions above 100 K. While a 300 K transition point may be far off in the future, materials with critical points above the boiling point of liquid nitrogen (77 K) hold great promise for driving down costs in commercially available and future technologies.

Scientists have yet to understand the exact mechanism underlying high-temperature superconductivity and believe it may require an entirely new theory beyond BCS. Yet it is apparent that the essential ingredient in these Type II ceramic materials is the presence of copper and oxygen. The three major families of high-temperature superconductors, Y-Ba-Cu-O (YBCO), Bi-Sr-Ca-Cu-O (BSCCO), and Tl-Ba-Ca-Cu-O (TBCCO), all contain copper-oxygen planes which are now widely presumed to be the preferred pathway of the superconducting current. Large-scale application of these materials has been limited by poor alignment and discontinuities of the copper-oxygen planes. Regions of poor alignment effectively present a smaller cross-sectional area through which the current can pass, resulting in a decrease in J_c. It is believed that increasing the superconducting grain alignment, or increasing "texture," serves to promote the alignment of the copper-oxygen planes and thereby provides a higher critical current property. A more detailed examination

of grain boundary impact on current flow is discussed in the work of Dimos and Chaudhari [5].

2.3 Surface Energy Driven Grain Alignment in the Bi-2212/Ag System

Previous research has demonstrated a high degree of BSCCO texture at the interface with a silver substrate after melt-processing of the precursor powder. The c-axis of the $Bi_2Sr_2Ca_1Cu_2O_x$ grain is preferentially normal to the plane of the Ag face, as shown in Figure 1.

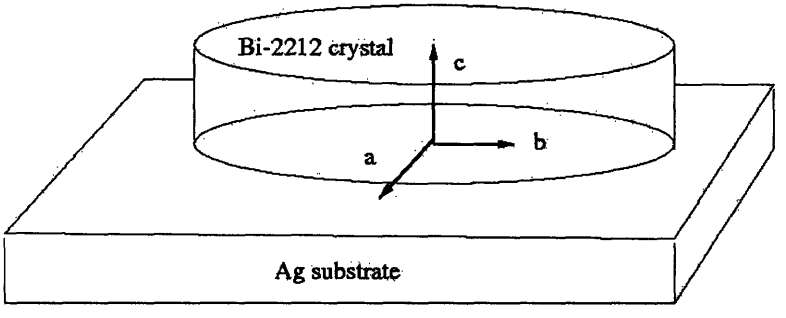

Figure 1: Platelet-like $Bi_2Sr_2Ca_1Cu_2O_x$ crystal with c-axis orthogonal to the Ag surface. This BSCCO phase is commonly known as "Bi-2212."

It has been experimentally observed that during melt-processing the growing superconductor crystals are somewhat mobile in the surrounding peritectic liquid and can rotate their alignment. A theoretical model provided by Cecchetti and Ferreira [6] suggests that it is energetically more favorable for a grain to align its c-axis perpendicular to the interface and it will rotate in the free liquid to do so. A simplified treatment of the model follows.

The model begins with a number of assumptions: that during melt-processing and solidification the superconductors grow heterogeneously on the substrate with no preferred

c-axis alignment (Figure 2); and that anisotropic crystal growth occurs preferentially in the *ab* plane (Figure 3), resulting in a platelet-like superconducting crystal.

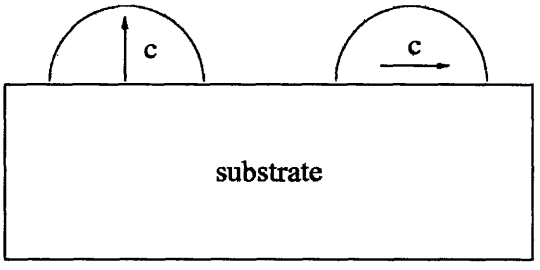

Figure 2: Heterogeneous nucleation of Bi-2212 crystals with no preferred c-axis direction.

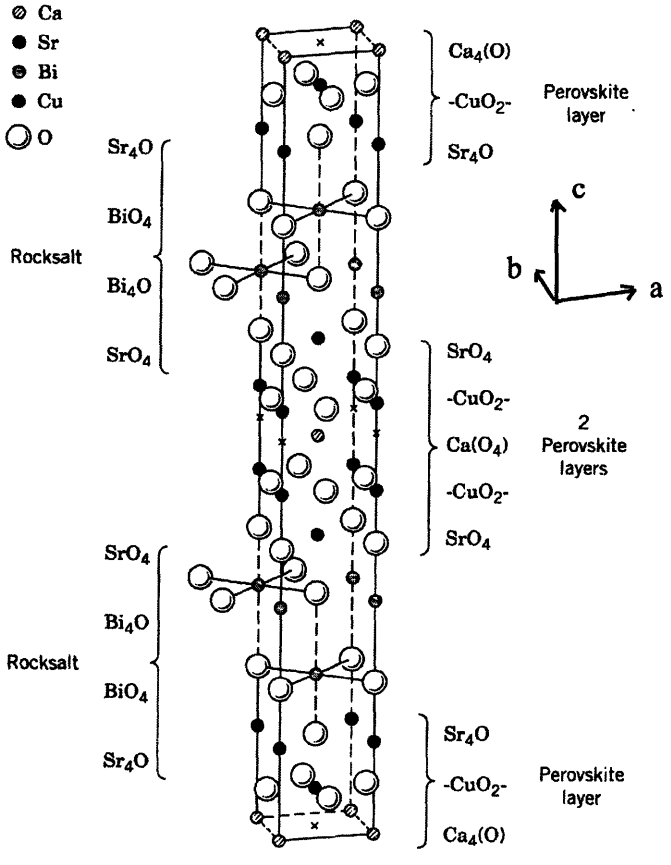

Figure 3: Bi-2212 crystal structure [7]. Grain growth preferentially occurs in the *ab* plane.

After a certain processing time, one would expect from the model assumptions the two types of grain orientation illustrated in Figure 4.

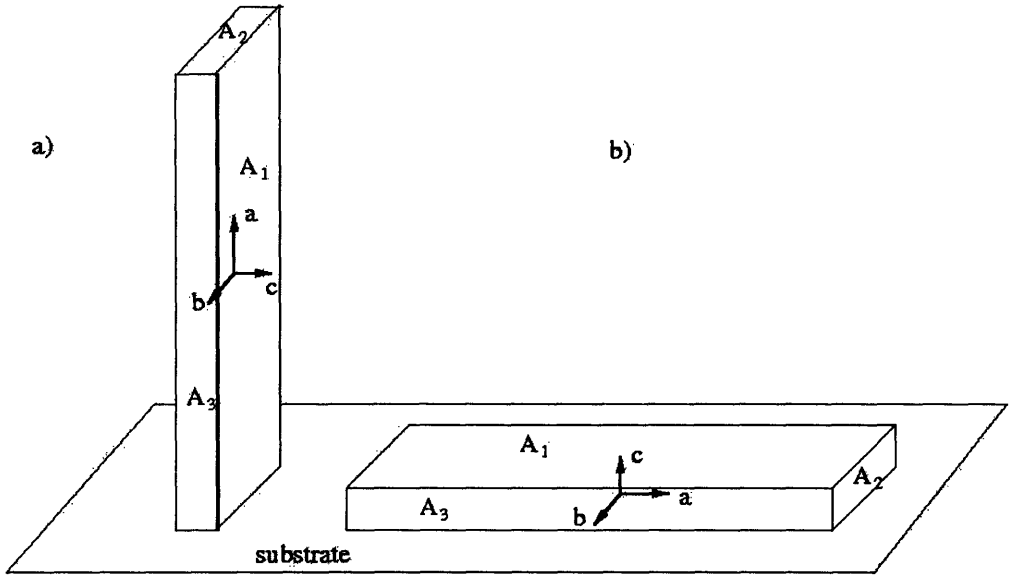

Figure 4: Two grain alignments resulting from the theoretical model assumptions. a) has its c-axis parallel to the substrate plane and b) has its c-axis normal to the substrate plane.

Experimentally it has been seen that the c-axis is highly probable to align normal to the interface as in Figure 4b. From this observation, it is stated in the model that the following equation can be written describing the surface energy interaction between the Bi-2212 plate-like crystal and any foreign plane:

$$A_1\gamma_{Bi/S} + 2A_2\gamma_{Bi/L} + 2A_3\gamma_{Bi/L} + A_1\gamma_{Bi/L} < 2A_1\gamma_{Bi/L} + A_2\gamma_{Bi/S} + A_2\gamma_{Bi/L} + 2A_3\gamma_{Bi/L} \quad (1)$$

where A_1-A_3 are the respective Bi-2212 crystal faces areas shown in Figure 4, γ

represents the surface energy per unit area, and the subscripts Bi/L and Bi/S indicate whether the interface is between the crystal and the peritectic liquid or the foreign substrate, respectively.

Equation (1) represents the total surface energy for each of the two orientations in Figure 4, implying the orientation having *c*-axis normal to the substrate plane has less total surface energy. Rearranging Equation (1) and canceling like terms leaves:

$$A_1\gamma_{Bi/S} + A_2\gamma_{Bi/L} < A_1\gamma_{Bi/L} + A_2\gamma_{Bi/S} \quad (2)$$

Experimental results show the anisotropic growth yields grain growth in the *a* and *b* directions 10-30 times larger than in the *c* direction [8-10]. It can then be assumed $A_1 >> A_2$, and the A_2 terms can be dropped, giving the end result:

$$\gamma_{Bi/S} < \gamma_{Bi/L} \quad (3)$$

Equation (3) suggests the A_1 face surface energy dominates the total crystal surface energy and that the Bi-2212 crystal minimizes its surface energy when its c-axis is normal to the foreign substrate. It follows that providing a flat Ag interface with which the superconducting grains can interact will enhance texturing as crystals grow at the surface.

Two other consequences of the model should be noted: first, that any foreign substance will provide a surface upon which the superconducting crystal will align its c-axis, thus arbitrarily shaped impurities or additional phases in the Bi-2212 layer will contribute to a decline in overall texturing; and second, that texturing will decrease as distance from the substrate interface increases, as local regions of aligned grains will nucleate in the free liquid, but will exhibit no orientation relation with respect to other locally aligned regions.

Chapter 3

Experimental Procedure

Our work was designed to provide further testing of the surface energy model by melt-processing Bi-2212 on a flat silver substrate. To combat the decrease in texturing far from the interface, we utilized a second flat Ag surface on top of the superconducting layer. We expected the upper Ag interface to provide texturing from the top-down in addition to the bottom-up texturing from the lower Ag surface. Provided the superconducting layer was not too thick—no more than approximately 20 microns—so as to minimize random local grain alignment in the middle, it was anticipated the two interfaces would provide a high degree of texture throughout the superconducting layer (Figure 5).

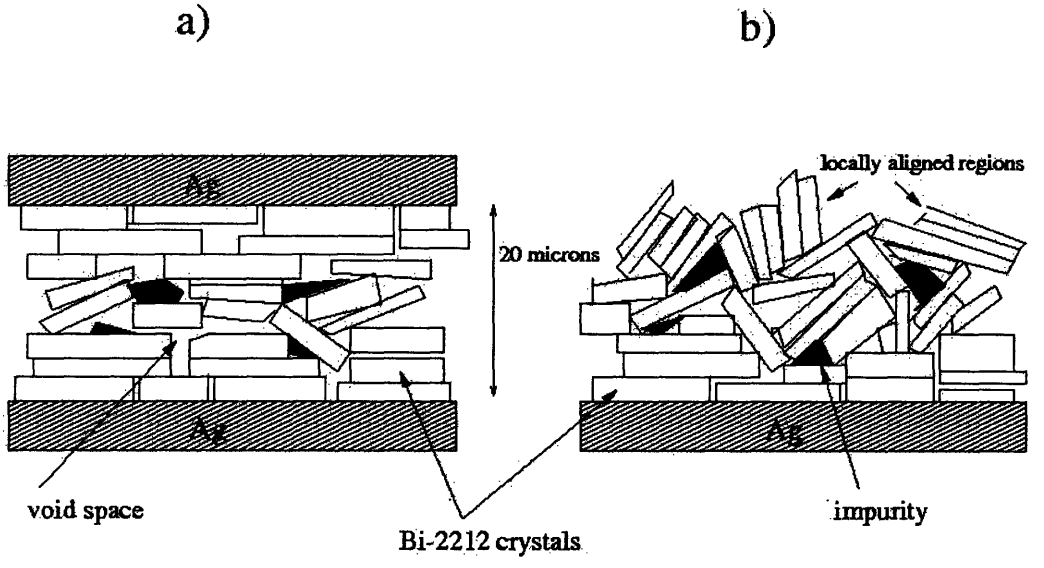

Figure 5: Second Ag interface effect. a) shows how a second Ag interface can provide consistent texturing throughout the BSCCO layer. b) reveals how a sample with only 1 Ag surface will have high alignment at the interface, but it may have locally aligned regions far from the Ag interface that do not exhibit long-range ordering. The sketches also demonstrate how the surfaces of randomly shaped impurities can influence grain misalignment.

We then sought to establish a relation between degree of texturing and the critical current, expecting higher grain alignment to provide improved J_c values.

3.1 Bi-2212 Sample Preparation and Melt-Processing

A commercially available 99% pure $Bi_2Sr_2Ca_1Cu_2O_{8.15}$ powder from Sigma-Aldrich was used for sample preparation. The BSCCO powder and isopropanol were combined in a ratio of 170 mg to 1.0 mL and set in an ultrasound bath for 10 minutes. The slurry was deposited on 50 micron-thick 99.9% pure Ag silver foil via glass pipette. Evaporation of the isopropanol left behind a thin film of BSCCO on the Ag surface. Sample dimensions were approximately 1 cm by 1 cm with a final melt-processed superconducting layer thickness of 20 ± 10 microns.

Our experimental methodology was to test "open-face" samples with only an underside layer of Ag and compare their properties to "closed-face" samples with the additional layer of Ag on top of the superconducting layer, creating a sandwich with the Bi-2212 between two silver sheets. To ensure high adherence between the top Ag foil and the Bi-2212 powder, a PR-22 pneumatic press was employed. Closed-face samples were pressed at 5250 Psi for a duration of 5 minutes at 190 °C. The elevated temperature determination was adopted from a previous work reporting increased J_c measurements in the BSCCO/Ag system for these processing conditions [11]. One closed-face sample did not undergo pressing and was processed after simply laying the top Ag surface on the BSCCO.

The melt-processing cycle also mirrored conditions in earlier studies, and the temperature versus time history is shown in Figure 6 [12]. The heat treatment consisted of a

partial melt stage induced at 880 °C, a cooling stage at a rate of 0.17 °C/min, and an isothermal annealing stage at 840 °C. A total of 10 samples were prepared in 3 different rounds of processing as shown in Table I.

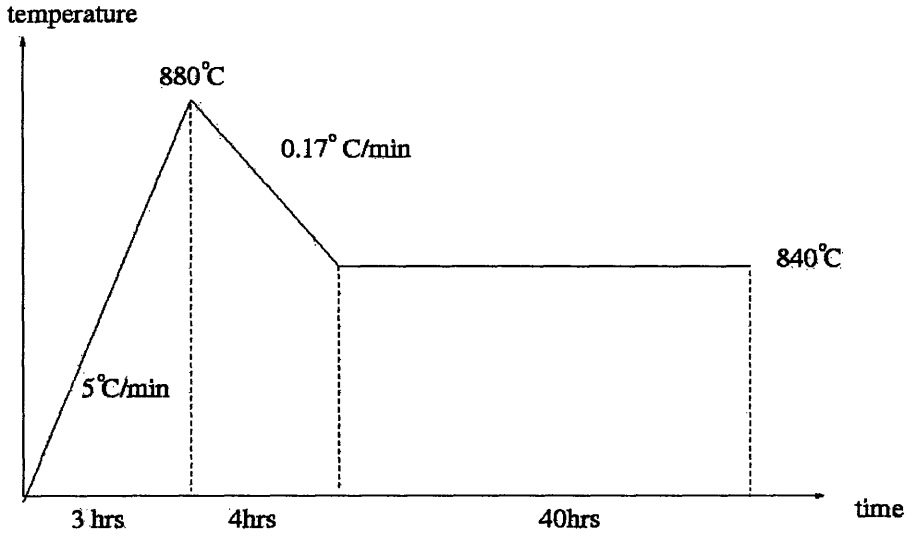

Figure 6: Melt-processing cycle for Bi-2212. Treatment has been experimentally observed elsewhere to optimize superconductor growth and minimize impurity formation.

Table I: Processing Conditions for the 10 Samples

Sample	Processing Round	Processing Type
1	Round A	Open-face
2		Open-face
3	Round B	Closed-pressed
4		Closed-pressed
5		Closed-pressed
6		Closed-pressed
7	Round C	Open-face
8		Closed-unpressed
9		Closed-pressed
10		Closed-pressed

Open-face samples contained only one Ag interface, whereas closed samples possessed two Ag interfaces. The pressed and unpressed notation reveals whether or not the sample underwent pneumatic pressing with the PR-22 apparatus.

3.2 Scanning Electron Microscopy

Microstructural observation was made using a CamScan Series 2 scanning electron microscope. Processed samples were cut in both the short and long transverse directions to allow a view of texturing in two directions (Figure 7).

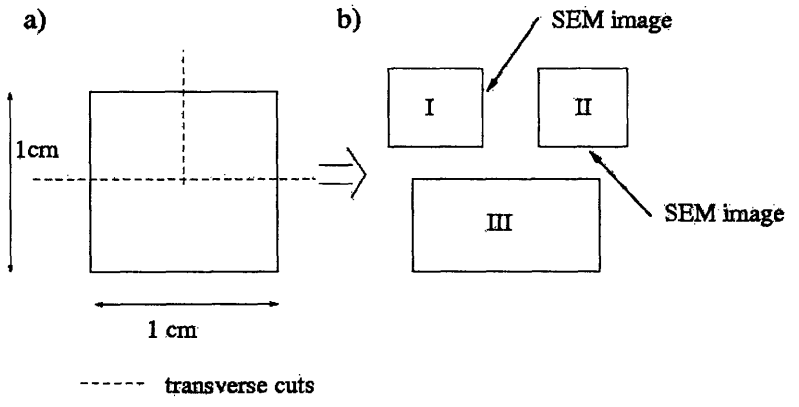

Figure 7: SEM sample preparation. a) Top view illustration of two transverse cuts on a processed sample producing sections I, II, III shown in b). Sections I and II were used for SEM analysis; section III was used for critical current testing and X-ray diffraction measurements.

A cold mount was prepared via an Epofix resin and hardener mixture, and the sample was polished to 0.05 μm using an Al_2O_3 grinding powder. Secondary electron emission was used for imaging.

3.3 Critical Current Measurement

Critical current measurements were performed in liquid helium to ensure the full superconducting state of Bi-2212, which has been observed to exhibit a T_c near 80 K. A

standard four-point probe technique provided a means to measure voltage across the sample while adjusting the current. A sketch of our experimental apparatus is shown in Figure 8.

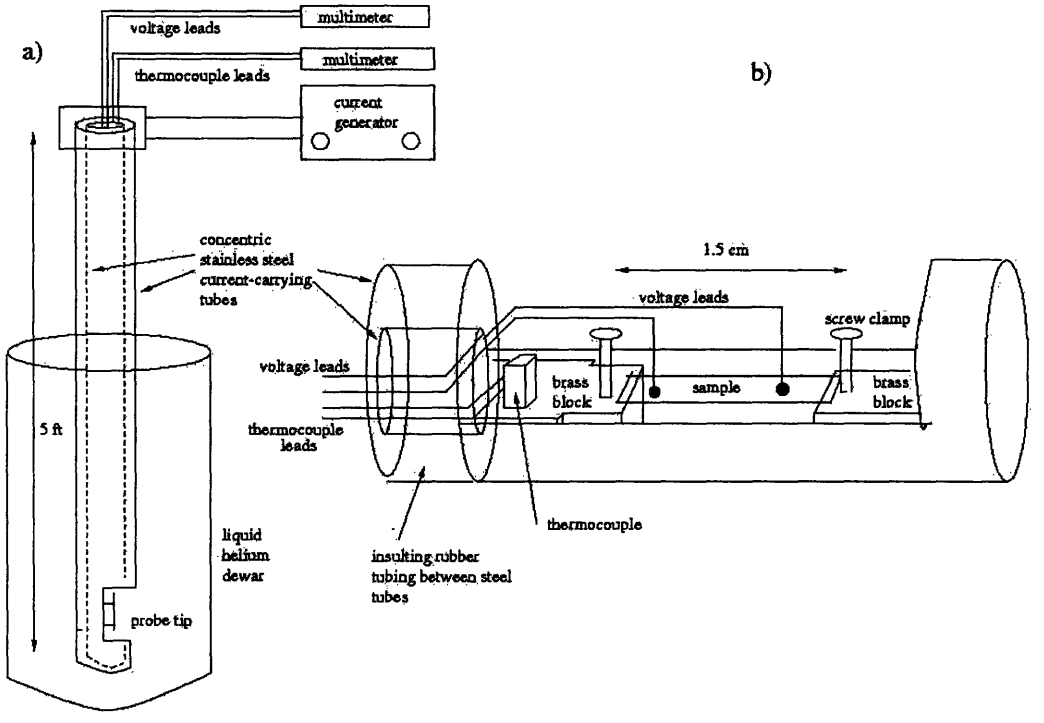

Figure 8: a) Schematic of the critical current test setup. Our probe was directly inserted into the liquid helium dewar. b) Magnified view of probe tip shows sample mounting on the assembly. Screw clamps secured the sample position.

A long, current-carrying probe consisting of two concentric stainless steel tubes was built for the measurements. Samples were mounted at the tip of the probe and voltage sensing leads were soldered to the sample Ag surface. Current could be adjusted manually and voltage measurements were taken on a digital multimeter with 0.1 μV accuracy, producing V-I plots for critical current determination.

The critical current, I_c, is a quantitative determination of when the material is no longer considered superconducting. There are three primary methods for calculating I_c (Figure 9).

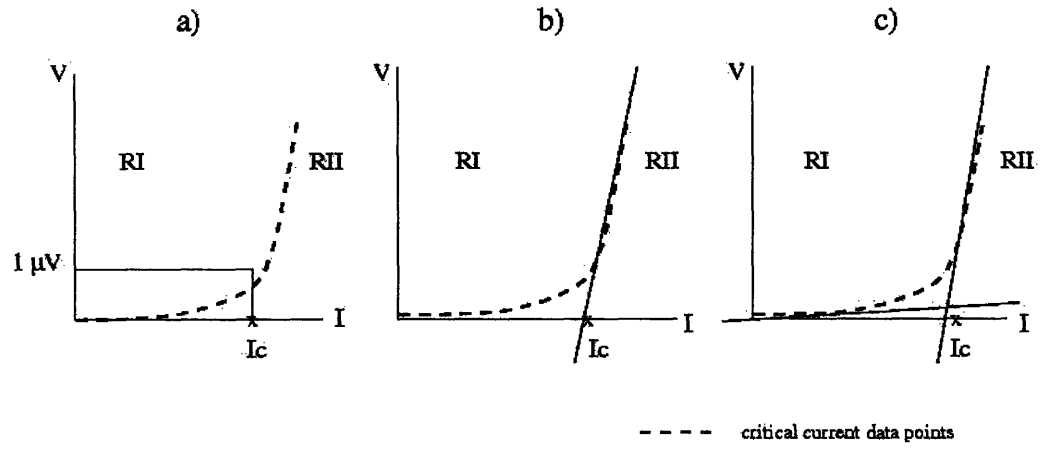

Figure 9: Three methods for calculating I_c. The 1 μV/cm criterion is demonstrated in a). Plots b) and c) represent two different linear extrapolation methods.

The first is to use a 1 μV/cm criterion, which presumes the material is in a non-superconductive state once the voltage drop exceeds 1 μV across a 1 cm section of the sample. The second and third methods are similar, requiring a linear fit of the data and an extrapolation of I_c. As shown in Figure 9b, method 2 uses a linear fit of the sharp rise in voltage in Region II and an extrapolation to 0 volts for I_c. The less conservative method 3 in Figure 9c employs a linear fit of both the rising voltage curve in Region II and the lower voltage points in Region I; the intersection of the two lines dropped down to 0 volts yields the I_c value.

For our experiments, the I_c for each sample was determined by the 1 μV/cm criterion in order to maintain consistency with the most widely sited method in literature. The useful quantity critical current density, J_c, defined as the I_c divided by the cross-sectional area of the superconducting layer, was calculated from an average layer thickness obtained by scanning electron microscopy.

3.4 X-ray Diffraction and Lotgering Factor

Microstructural analysis of the superconducting grain alignment was performed via X-ray diffraction. A Rigaku 300 X-ray diffractometer was used to perform X-ray measurements, using Cu K_α X-rays at 50 kV and 200 mA with a scanning rate of 10°/minute.

Lotgering introduced a method to quantitatively determine the degree of c-axis alignment in polycrystalline materials using the X-ray diffraction (XRD) technique [13]. When exposed to X-rays, a polycrystalline material with perfect c-axis alignment will cause constructive interference only for reflections from the (00*l*) planes. The same material with a random arrangement of crystals will produce reflections from all (*hkl*) planes.

Lotgering stated a comparison of the peak intensity sums for a randomly aligned material with a sample exhibiting some preferred orientation will yield a quantitative measure of the alignment. The Lotgering factor, F, can be calculated from the XRD spectrum as:

$$F = \frac{P - P_0}{1 - P_0} \tag{4}$$

where P is the integrated sum of all intensities, I, from (00*l*) reflections divided by the integrated intensity sum from all (*hkl*) planes, denoted as:

$$P = \frac{\Sigma I_{(00l)}}{\Sigma I_{(hkl)}} \tag{5}$$

and P_0 represents the same quantity for a randomly-oriented sample. From this definition, a sample with F = 1 has perfect c-axis alignment, and a sample manifesting F = 0 is perfectly random. It was believed in our experiment that open-face samples would show less c-axis alignment than closed-pressed samples, and therefore evidence a lower F.

Preparation of the powder sample for X-ray diffraction was achieved by combining the Aldrich 99% $Bi_2Sr_2Ca_1Cu_2O_{8.15}$ powder with collodion adhesive gel in a ceramic crucible. The slurry was mixed in the crucible and then smeared on a glass microscope slide surface. The mounting was placed in a furnace at 80 °C to allow the glue to set. Open-face specimens were ready for XRD by adhering the underside Ag layer to a glass microscope slide. Closed-pressed samples were delaminated following critical current measurements to expose the superconducting grains and then similarly adhered to a microscope slide mounting.

For our analysis, the (00*l*) planes were the (002), (004), (006), (008), (0010), (0012), (0014), (0016), (0020), (0026), and (0028) planes. The (*hkl*) planes were comprised of all the (00*l*) planes plus the (111), (117), (020), (022), (0210), (1113), (1115), (228), (2210) planes. Jade analysis software [14] was used to subtract background intensity from X-ray spectra and integrate peak intensities to calculate Lotgering factors.

Chapter 4

Results

4.1 Critical Current Measurement

Representative critical current plots for an open-face sample and a closed-pressed sample are shown in Figure 10. Both V-I plots exhibit a number of data points for low current that produce zero voltage, indicating the material is in a superconducting state with zero resistance. The voltage starts to increase monatomically as the current is raised, in accordance with the continuous transition of vortex motion discussed in Section 2.1.

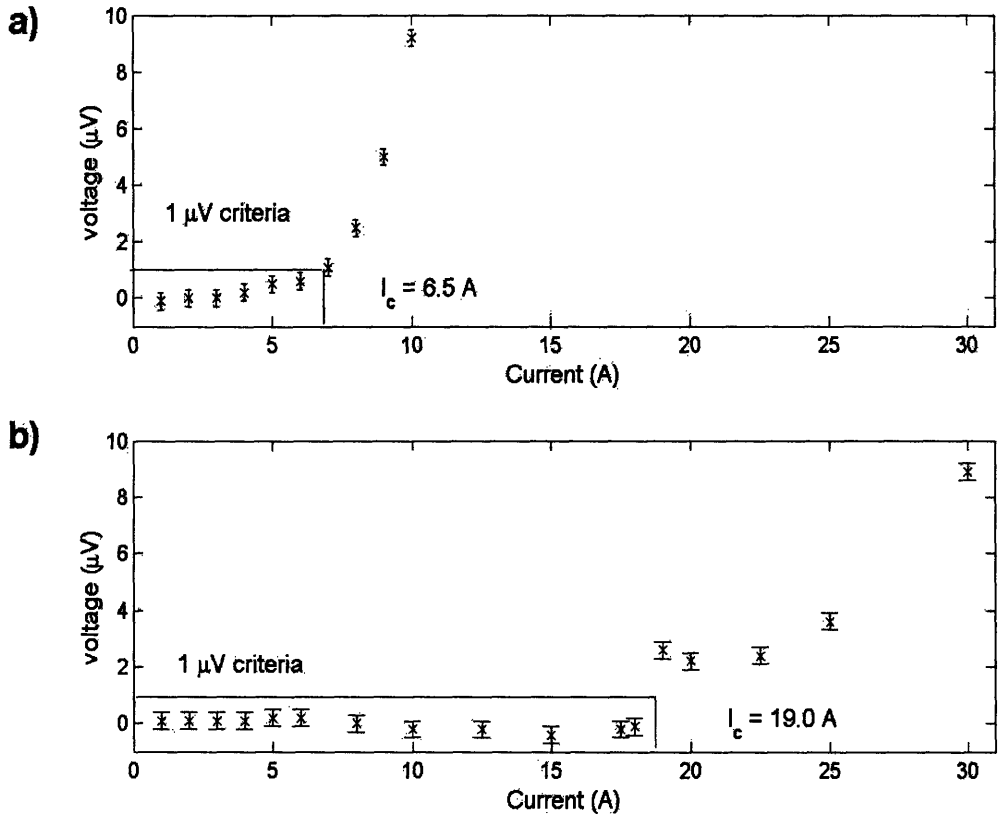

Figure 10: Critical current V-I plots of open-face Sample 7 (a) and closed-pressed Sample 9 (b) where I_c was determined using the 1 μV/cm criterion.

The 1 μV/cm criterion provided a standardized way to determine when the material was no longer superconducting, although it is important to recognize this criterion is somewhat arbitrary. In Figure 10a is it clear there is a finite voltage at a current of 5.0 A, implying our sample is no longer perfectly superconducting. The sharpness of the transition between zero resistance and finite resistance also varied for each sample; Figure 10b illustrates a case with sharp transition. The two cases shown manifest a three-fold increase in I_c for a closed-pressed sample against an open-face sample.

Scanning electron microscopy offered a qualitative means to measure the average thickness of the superconducting layer. The superconducting layers were generally 15-20 microns thick, with a variation of no more than 10 microns across the full length of the sample (Figure 11).

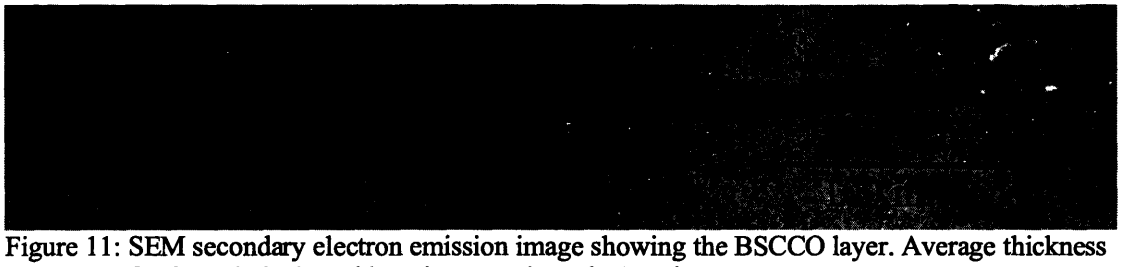

Figure 11: SEM secondary electron emission image showing the BSCCO layer. Average thickness for Sample 3 viewed here is approximately 15 microns.

The critical current density J_c was calculated after computing the cross-sectional area for each sample. Results for all samples are displayed in Figure 12.

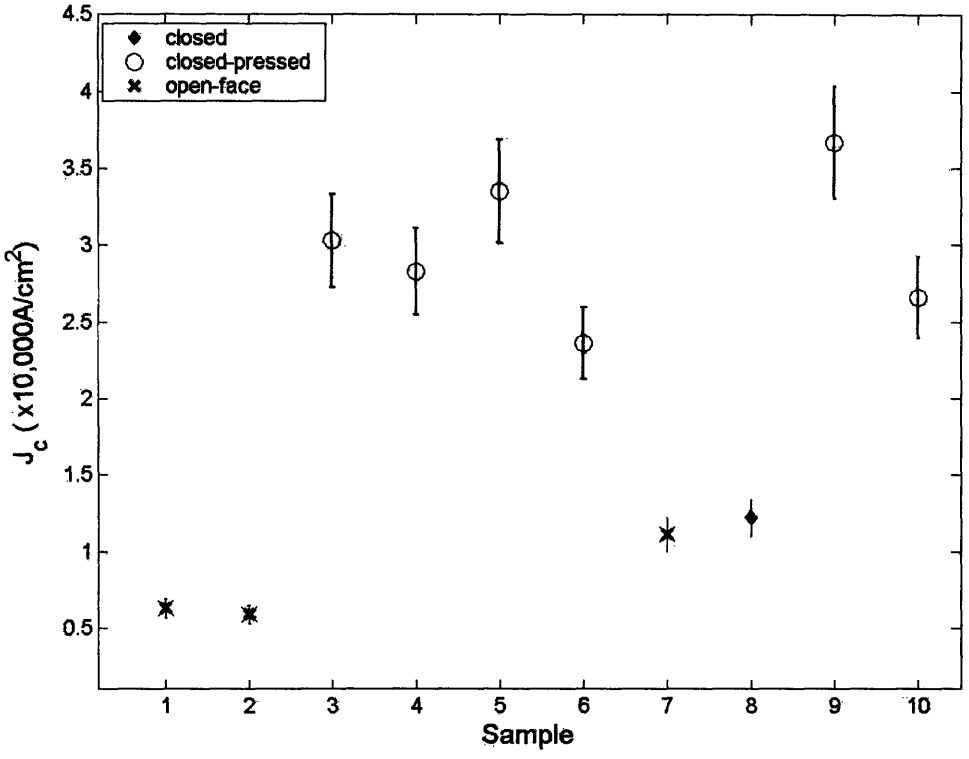

Figure 12: Plot of J_c versus sample for open-face, closed, and closed-pressed processing. Errorbars were calculated from taking a second critical current measurement for one sample and recalculating the J_c. A 10% change in J_c was observed and this deviation was applied to each measured critical current. The errors on samples 1 and 2 are difficult to resolve on the plot.

Figure 12 shows a 3 to 6 fold increase in J_c values for the closed samples when compared to the open-face samples, with a maximum range of 5,900 A/cm^2 to 36,700 A/cm^2. The increase in current density for closed-pressed samples over an unpressed closed sample also suggests the additional processing step of using a pneumatic device press to seal the top Ag layer on the BSSCO improves the superconducting property.

4.2 X-ray Diffraction

The Lotgering Factor made available a characterization technique to quantify the degree of Bi-2212 grain alignment in each sample, allowing a study of the processing-microstructure relationship. Figure 13 displays the X-ray diffraction pattern for the randomly-orientated powder sample and a textured closed-pressed sample.

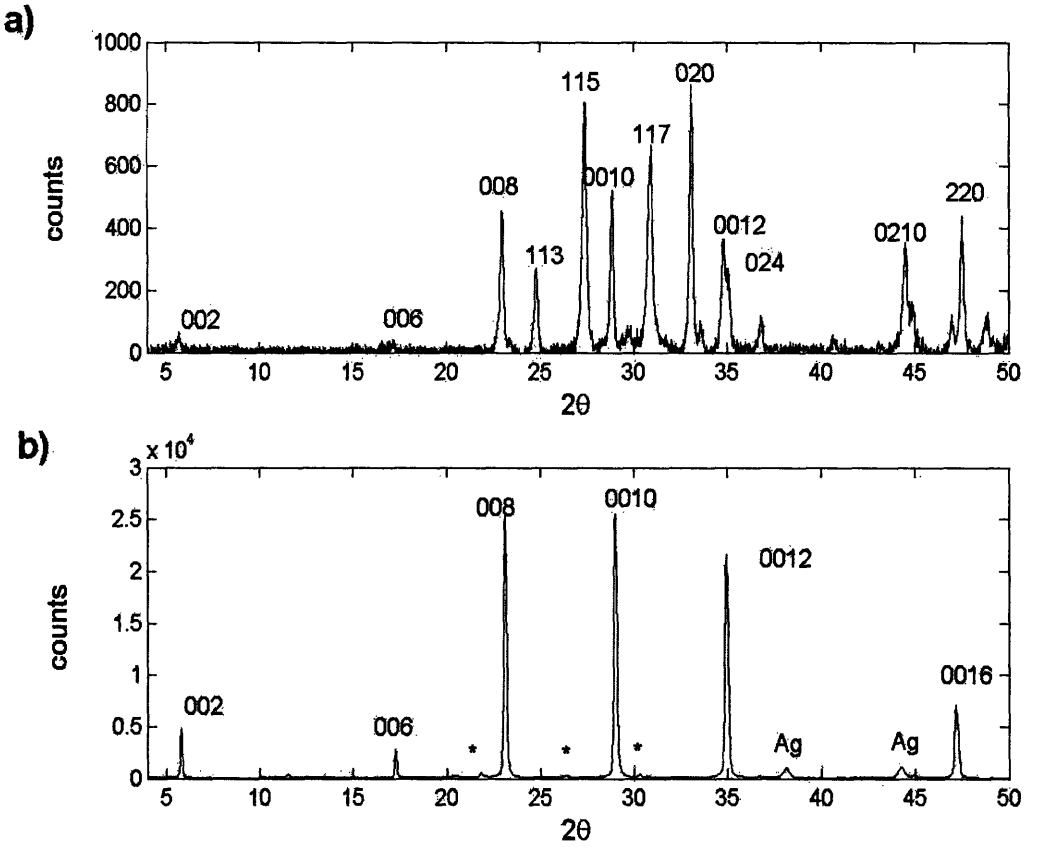

Figure 13: X-ray diffraction patterns of the randomly-oriented powder (a) and textured Sample 3 (b) showing strong (00*l*) peaks. Impurity peaks are labeled with the symbol (*).

Our experimental peaks for the powder sample accurately correspond with the known peaks of Bi-2212. The presence of impurity peaks is expected, as our powder contains 1% non-Bi-2212 substances and the melt-processing conditions allow for

secondary phase and impurity formation. A P_0 value from Equation (4) for the random sample to be used for all F factor calculations was found to be 0.185.

The spectrum in Figure 13b evidences strong (00*l*) peaks and greatly suppressed *(hlk)* peaks compared to the powder specimen, which implies a high degree of c-axis preferential alignment orthogonal to the Ag surface. The P value in Equation (4) for Sample 3 was calculated to be 0.874. A corresponding F = 0.845 suggests a highly textured specimen. F factors for all samples are contained in Figure 14.

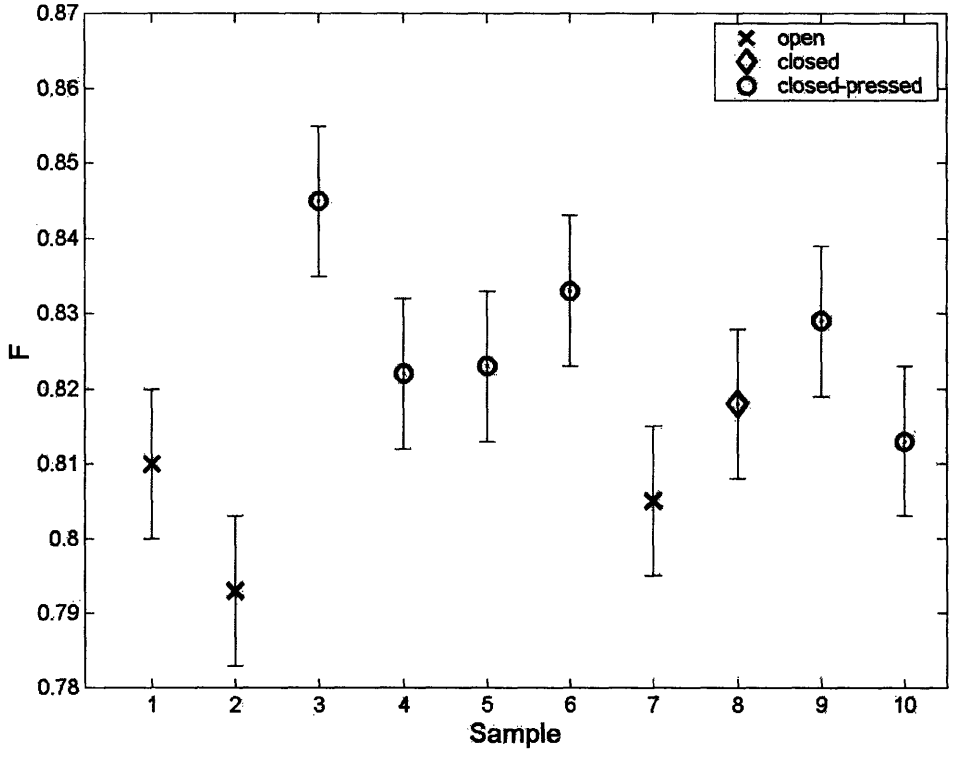

Figure 14: F vs. sample. The error analysis is discussed in the section 5.2

The results show a correlation between processing and microstructure with closed samples exhibiting higher F factors than open samples, implying enhanced texture. It should be noted that the unpressed closed sample falls roughly between the open-face and closed-pressed values.

Chapter 5

Discussion

5.1 Critical Current and Lotgering Factor Correlation

A full determination of the relation between processing, microstructure, and property for our experiment with the Bi-2212/Ag system can be performed by plotting the Lotgering factor against critical current density, as displayed in Figure 15.

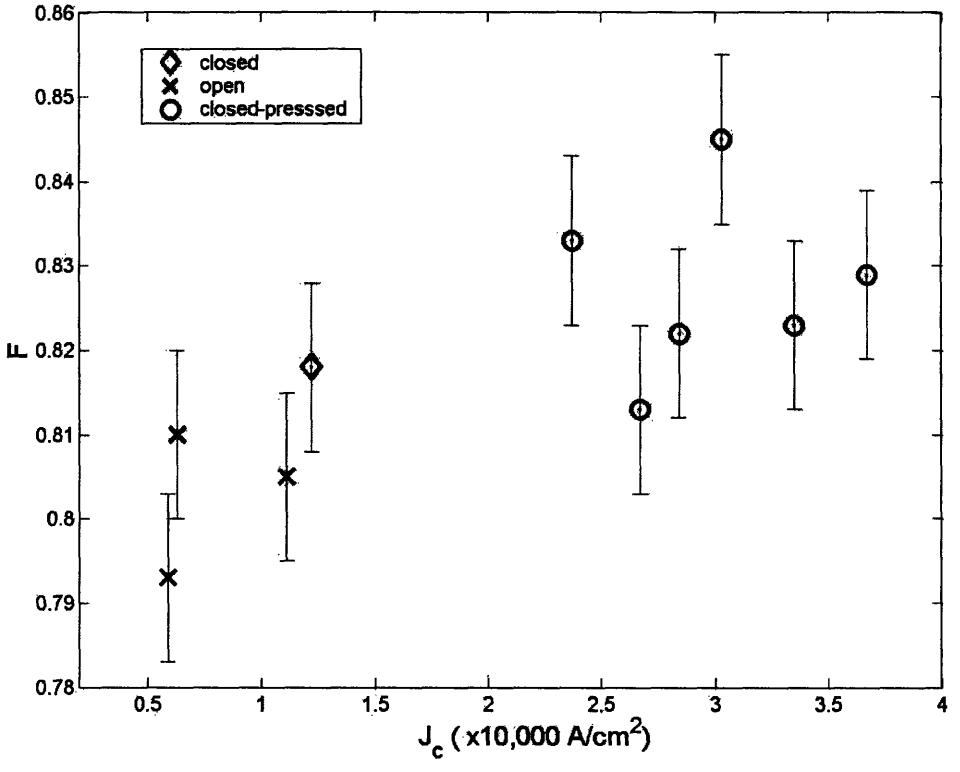

Figure 15: F vs. J_c for all processed samples.

The data in Figure 15 suggests that samples with a higher critical current density exhibit a higher degree of c-axis orientation, and therefore possess better grain alignment. The plot

further reveals that the samples with the larger J_c values were processed with the second Ag interface pneumatically pressed on top of the superconducting layer. It is evident that the unpressed closed sample has a J_c lower than the closed-pressed samples and higher than the open samples, and that the F factor falls near the middle—both as expected. Although more closed samples would be needed to make a statistically relevant determination, our one closed sample lends weight to the idea that pressing creates improved contact with the Bi-2212 layer, leading to higher texture.

The results support the surface energy model that a flat foreign substrate provides a means for c-axis grain alignment in Bi-2212. In our case, the upper Ag thin foil provides a second interface upon which crystals can align, resulting in a high degree of texture of the thin superconducting layer between the two Ag surfaces. Conversely, a single underside Ag surface provides texture development only at the bottom interface and grain alignment diminishes as distance from the surface increases. As a consequence, the closed-pressed samples have enhanced overall texture. Our results further support the idea that improved microstructure in the form of higher texture yields a better critical current property by ensuring copper-oxygen plane connectivity.

While it is clear that there is a difference between open-face and closed-pressed critical current density values, a major question still arises from the discrepancy between J_c values of similarly processed samples. For example, one needs to account for the near 10,000 A/cm^2 increase in J_c for Sample 9 compared to the identically processed Sample 10.

A number of factors can contribute to the disparity in J_c between samples. We observed in SEM analysis that texturing was non-uniform throughout the superconducting layer, as displayed in Figure 16.

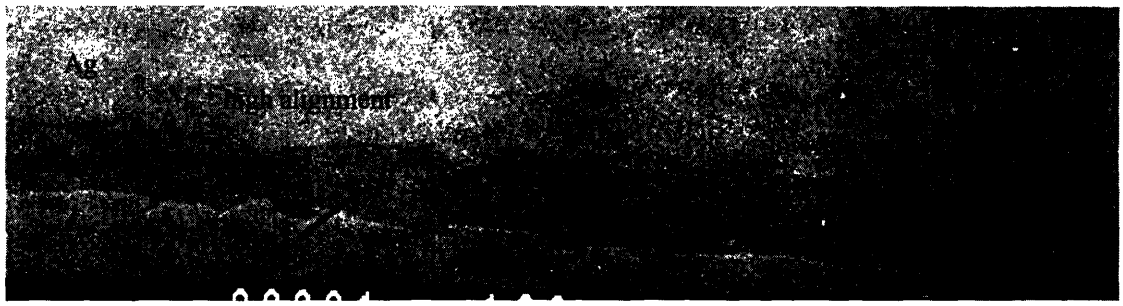

Figure 16: Secondary electron emission SEM image of Sample 3 showing local regions of high and low alignment. The non-perfect alignment qualitatively corroborates with an F of 0.845.

It follows that there exist local regions of high alignment and poor alignment scattered through the sample. The geometric arrangement of these regions can dictate the critical current by presenting an effectively smaller window for the current to pass through, shown in Figure 17.

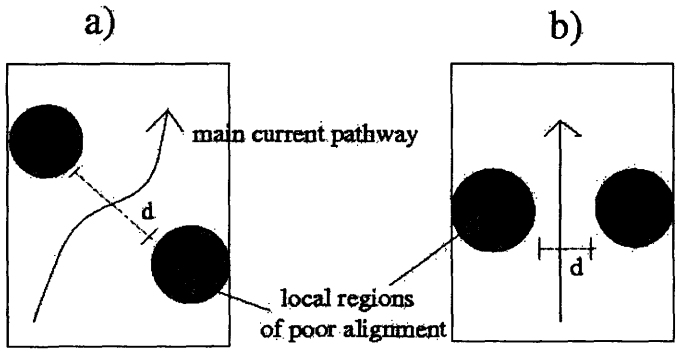

Figure 17: Example of geometric configuration of low texture regions. The picture illustrates how arrangement of low texture regions can affect critical current density by providing a smaller effective current pathway window *d*.

A similar F factor may be observed for the samples as the ratio of high texture to low texture regions is the same, but J_c may vary widely due to their positioning. Another characterization technique requiring a planar view is necessary to determine the location of region alignment and quantify this effect on J_c. It is likely that an imperfectly flat Ag surface with slight depressions, crevices, grooves, or bumps will create local nucleation

sites with poor alignment. The density, degree of deformation, and configuration of these defects will play a role in the critical current property for each sample.

SEM analysis further revealed a non-uniform thickness of the BSCCO layer, which may be due to uneven slurry deposition. The average superconducting thickness was 15-20 microns, but fluctuated by up to 10 microns. We observed that beyond a certain critical thickness of approximately 20 microns, the grain alignment is noticeably reduced away from the interfaces; this is consistent with Figure 5 where one can envision low alignment in the middle region if the Ag plates are too far apart. The fluctuations in thickness could therefore additionally lead to local areas of poor texturing. It was attempted to process samples with thinner BSCCO layers, but this method led to some regions with no superconductor layer.

A dissimilarity in J_c values can also be caused by impurities or secondary phases created during the processing cycle. These impurities offer surfaces on which alignment can occur, but their often arbitrary shape leads to grain orientation in all directions (Figure 18). Further, their presence interrupts copper-oxygen plane connectivity and inhibits current flow.

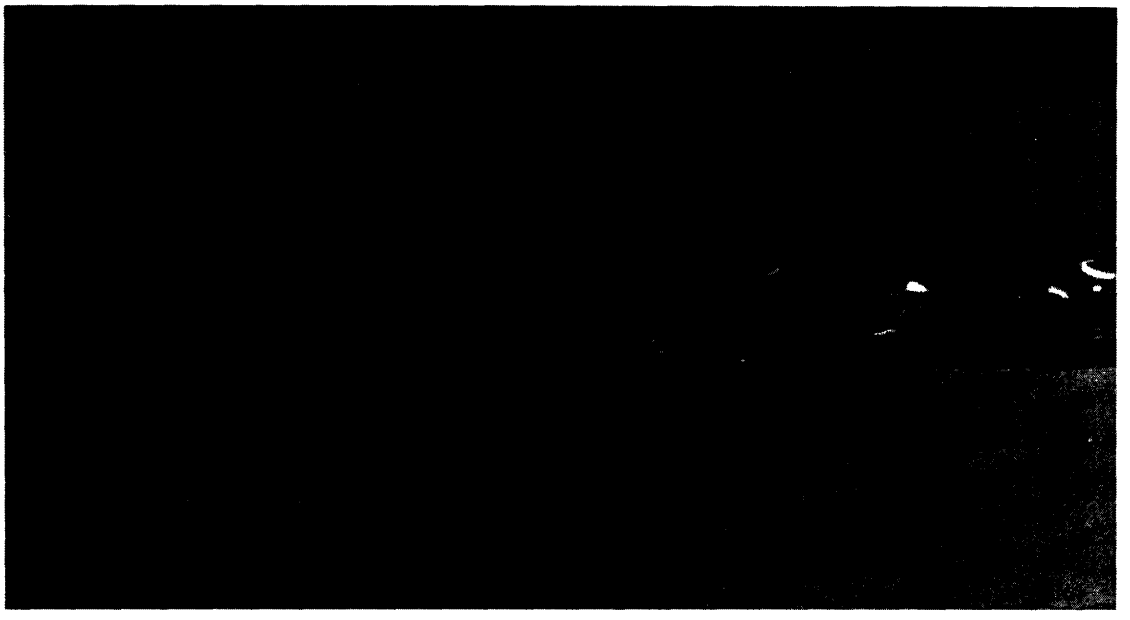

Figure 18: Secondary electron SEM image showing grain misalignment due to impurities and voids.

XRD spectra verify that different impurities and phases exist in samples processed in the same round (Figure 19). This effect might be caused by fluctuations in furnace temperature during melt-processing. It was experimentally determined that the furnace temperature varied by a few degrees at the 880 °C peak and varied spatially throughout the interior. It is known that even a 1 degree imprecision in temperature control or slight changes in atmospheric conditions can dictate impurity phase formation. The exact placement of each sample in the furnace and different atmospheric processing conditions for each round could thus contribute to different impurity growth environments. The types of non-Bi-2212 phases and their relative abundance that result from these irregular environments will ultimately affect J_c.

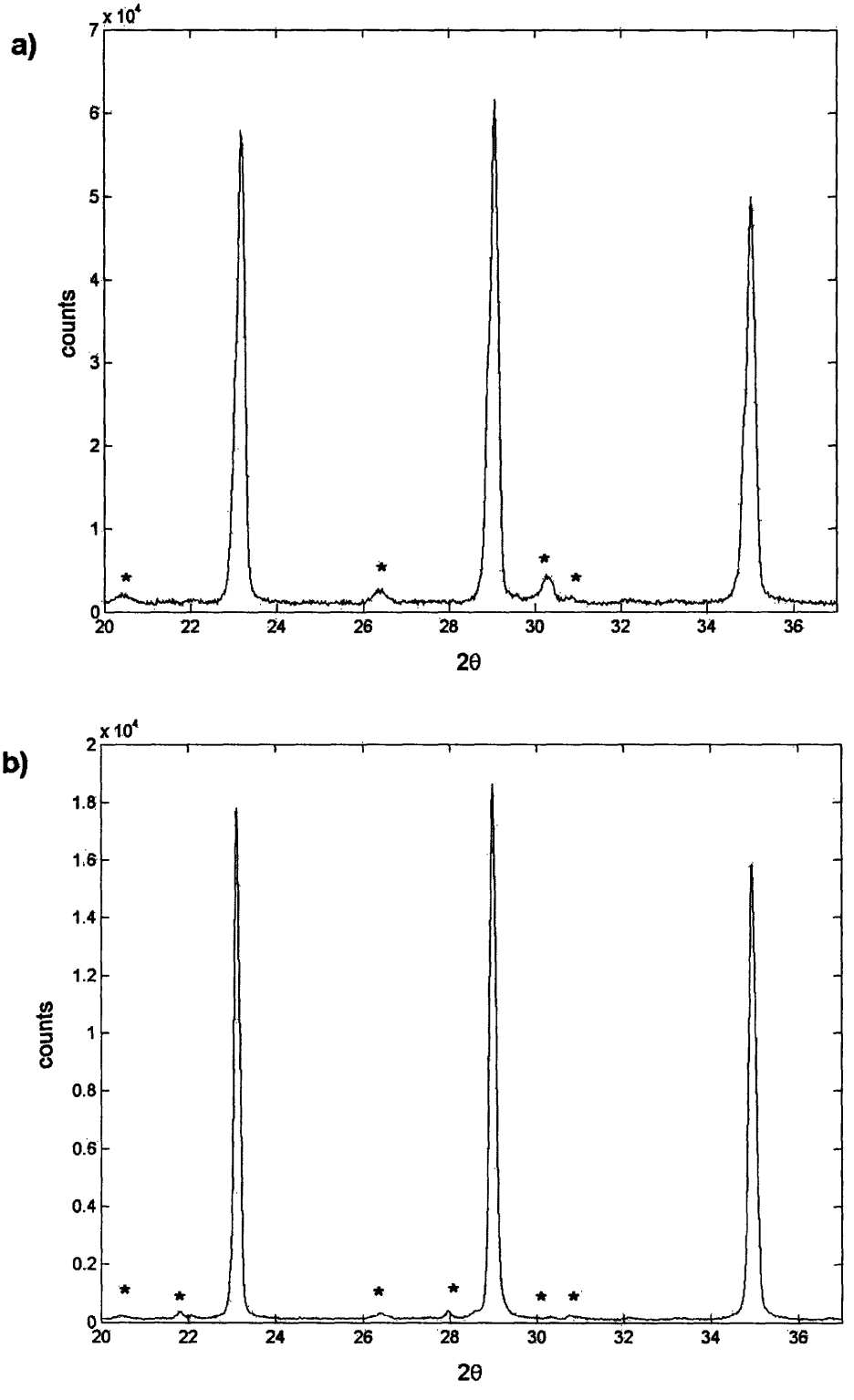

Figure 19: XRD spectra for Sample 7 (a) and Sample 10 (b) illustrating the difference in the presence and relative abundance of impurity peaks (*) for processing Round 3.

5.2 Error Analysis for Lotgering Factor

The error on the Lotgering factor was calculated in three different ways: 1) by including and discounting peaks in the $\Sigma I_{(hkl)}$ term from Equation (5) that ambiguously originated from either Bi-2212 or an impurity; 2) by redoing the intensity summations for both the powder sample and a textured sample; 3) by retaking the XRD spectrum of a sample and performing the analysis a second time.

Method 3 produced a small error of ± 0.005 and method 2 produced a slightly larger deviation of approximately ± 0.01. Method 1 yielded errors between ± 0.01 and ± 0.07, depending on the number and intensity of peaks that were incorrectly incorporated. We chose for method 1 an error of ± 0.025, representing a roughly 20% variation of the total intensity in the $\Sigma I_{(hkl)}$ term due to incorrectly incorporated or discounted peaks. This conservative estimate was selected due to the high number of impurity phases possible and their complex crystal structures which both give rise to a large number of peaks.

We chose an F factor error of ± 0.01 to use for our data as we felt it most accurately represented the true sample error, believing the other analysis methods too conservative or too optimistic. Figure 20 displays a comparison of the errors for method 1 and method 3.

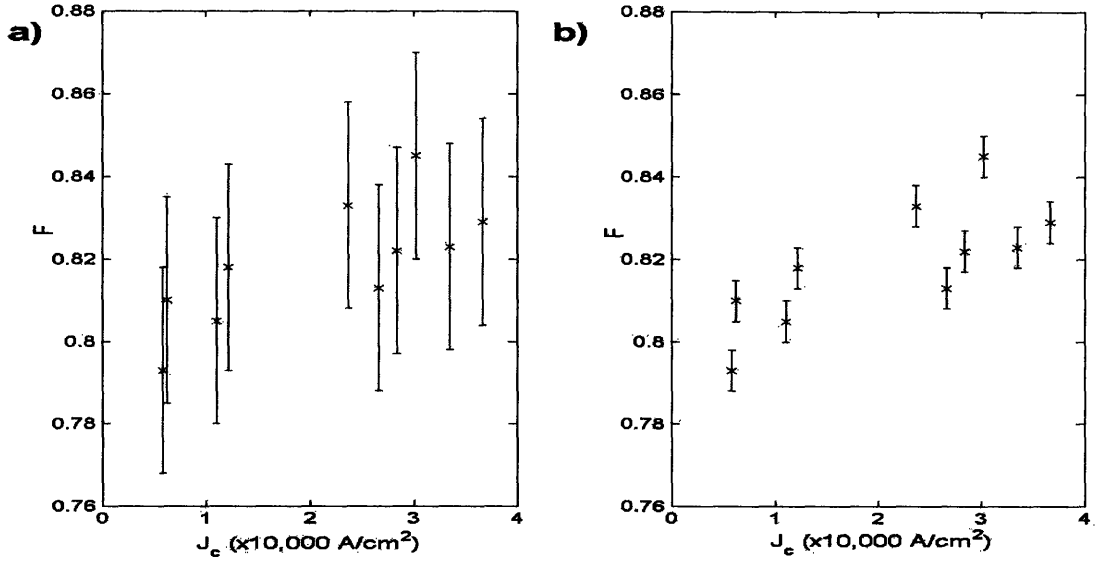

Figure 20: F vs. J_c for different errorbar calculations. a) shows errorbars of ±0.025 from the highly conservative method 1. b) shows errorbars of ±0.005 from method 3. Figure 15 shows the error bars of ±0.01 that we chose for our measurements.

5.3 Extrapolation to Higher J_c Values

Our data for the F factor plotted against critical current density appeared relatively linear and a regression fit was preformed in Matlab (Figure 19). Using the linear fit equation, J_c values can be extrapolated for higher F factors. An F = 0.90 would yield a J_c of 105,000 A/cm^2, and an F= 0.95 would give a J_c of 158,000 A/cm^2. It is possible that a linear relation does not describe the correspondence between J_c and F, but the extrapolated J_c values are certainly physically reasonable.

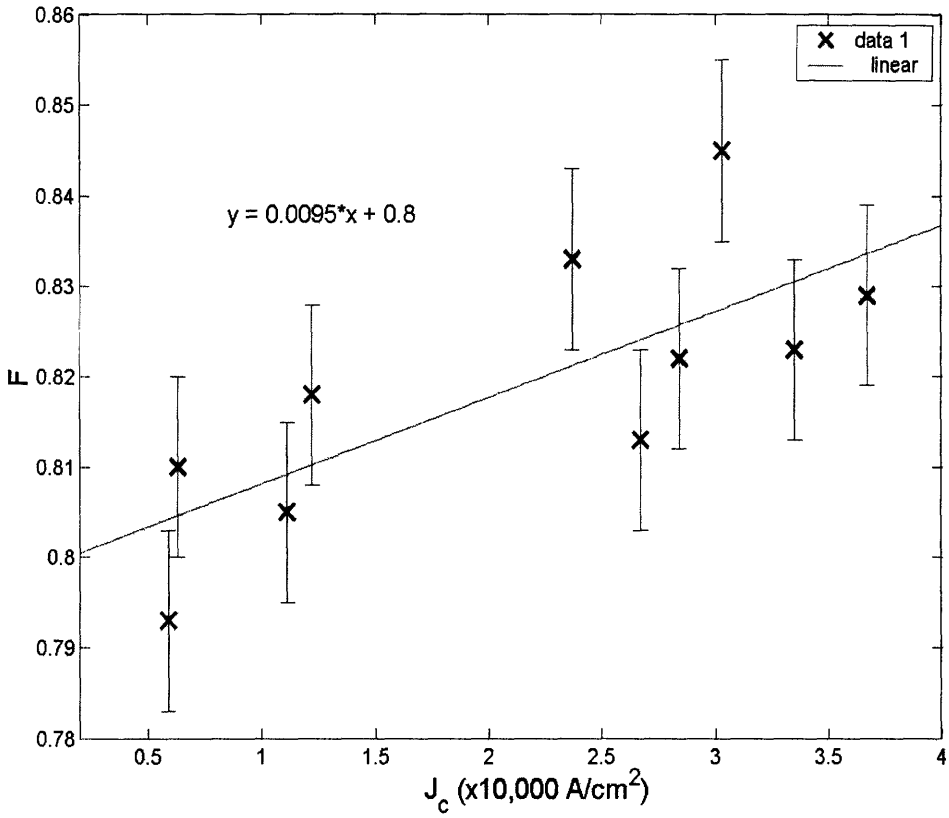

Figure 21: F vs. J_c with linear fit.

Chapter 6

Conclusions

Our results demonstrate that there exists a clear connection between processing and critical current property in the high-temperature superconducting $Bi_2Sr_2Ca_1Cu_2O_x$ /Ag system. Samples with a second pneumatically pressed Ag interface showed an average critical current density, J_c, 3.8 times greater than samples with only a single underside Ag layer, providing experimental support of the surface energy driven grain alignment theory. An unpressed closed sample possessed a J_c in between the open-face and close-pressed specimens, which implied pressing increases texturing by forming an improved Ag/Bi-2212 interface with less gaps and voids; however, more closed-unpressed samples are required for better statistics.

We additionally quantitatively measured a relation between processing and microstructure via the Lotgering factor, F, a quantity calculated from X-ray diffraction that gives an indication of c-axis alignment. F factors calculated for closed-pressed samples were slightly higher than their open-face counterparts, revealing a stronger grain alignment. A comparison of F and J_c illustrates that a higher degree of texturing correlated with improved superconductor performance, linking together the interfacial energy considerations of processing, the microstructural analysis of grain alignment, and the material critical current property.

A wide disparity in J_c values between individual closed-pressed samples was observed. It is believed the configuration of local regions of high and low texture throughout the BSCCO layer plays a role in determining critical current. Such regions may be the result of deformities in the Ag surface or non-uniform slurry deposition, which are

both conditions unique to each sample. Impurities and secondary phases formed during melt-processing also affect J_c. Small temperature fluctuations during the heat treatment cycle between processing rounds and the spatially-dependent temperature in the furnace could promote the growth of different impurities, leading to varied superconducting properties.

Chapter 7

Suggestions for Future Research

For further testing we would like to find a method to quantify regions of high and low texturing throughout the Bi-2212 layer and determine if a correlation exists with critical current density. We also seek to characterize the different types and relative abundance of secondary phases and impurities in each sample and investigate their link with critical current. A third area of interest would be to see if higher F factor samples obey a linear relation with J_c.

Bibliography

[1] Bardeen J, Cooper L N, Schrieffer J R 1957 *Phys. Rev.* **108** 1175

[2] Chaddah P 2003 *Sadhana* (India) **28** 273

[3] Campbell A M and Evetts J E 1972 *Adv. Phys.* **21** 199

[4] Bednorz J G and Müller K A 1986 *Z. Physik B* **64** 189

[5] Dimos D and Chaudhari P 1990 *Phys. Rev. B* **41** 4038

[6] Cecchetti E, Ferreira P J, Vander Sande J B 2000 *Supercond. Sci. Technol.* **13** 1270

[7] Chiang Y M, Birnie D, Kingery W D, *Physical Ceramics*, John Wiley and Sons, New York, 1997.

[8] Demyanec L N, Byikov A B, Kanunnikov G V, Melnikov O K, Androno A N and Khodan A N 1989 *Supercond. Phys. Chem. Technol.* **2** 169

[9] Yan Y, Kirk M A and Evetts J E 1997 *J. Mater. Res.* **12** 3009

[10] Hasegawa T, Kobayashi, H, Kumakura H and Togano k 1994 *Supercond. Sci. Technol.* **7** 579

[11] Gao W and Vander Sande J B 1992 *Supercond. Sci. Technol.* **5** 318

[12] Cecchetti E, Ferreira P J, Vander Sande J B 2000 *Physica C* **336** 192

[13] Lotgering F K 1959 *J. Inorg. Nucl. Chem.* **9** 113

[14] JADE 7-XRD Pattern Processing, Identification, and Quantification; Materials Data, Inc. 2004